Supercapacitors Prepared from Melamine-Based Carbon

Denisa Hulicova,* Junya Yamashita, Yasushi Soneda, Hiroaki Hatori, and Masaya Kodama

Energy Storage Materials Group, Energy Technology Research Institute, National Institute of Advanced Industrial Science and Technology, 16-1 Onogawa, Tsukuba, Ibaraki 305-8569, Japan

Received April 25, 2004. Revised Manuscript Received December 6, 2004

The electrochemical performance of supercapacitors made of a carbon material with a moderate amount of nitrogen atoms embedded in a carbon matrix is reported. Melamine was polymerized in the interlayer spaces of mica and afterward carbonized at various temperatures between 650 and 1000 °C. Elemental analysis and an XPS study showed that the nitrogen content of samples stabilized at 250 °C for 4 h prior to carbonization was generally higher if compared to their nonstabilized counterparts and that the nitrogen species were located preferably at the edges of graphene sheets. To understand the relationship between the capacitive performance and the porosity of stabilized and nonstabilized samples, the nitrogen adsorption/desorption method was also employed. Supercapacitors with the electrodes manufactured from these carbon materials showed a very good capacitive performance in 1 M sulfuric acid. The maximum gravimetric specific capacitance of 204.8 F g^{-1} was obtained from a sample carbonized at 750 °C. Specific capacitances per surface area were also calculated, and, as a result, the stabilized samples provided higher values than the nonstabilized samples, for example, 3.66 F m^{-2} for a sample stabilized and carbonized at 1000 °C. We associate the high values of capacitances in sulfuric acid with the pseudocapacitance that originates from an interaction between the nitrogen species and the protons of the electrolyte. This claim was verified by another measurement, where a neutral electrolyte (3 M NaCl) was used instead of sulfuric acid. We observed a decrease in capacitance with the surface area, and the values of capacitances per surface area were close to the values for activated carbons. Thus, the capacitance in NaCl can be attributed to the electrostatic interaction of ions on the double-layer rather than the pseudocapacitive interaction.

In recent years, supercapacitors have attracted considerable attention as alternative energy-storage systems. Activated carbon is the most frequently used electrode material for supercapacitors.[1,2] The storage of electric charges is mainly non-Faradaic, and the accumulation of ionic charges occurs on a double-layer at the electrode/electrolyte interface.[3] The large specific surface area and the porosity of the activated carbon are the basic requirements to achieve the quick formation of a double-layer which results in a high power density and long durability of these supercapacitors, termed also electric double-layer capacitors (EDLC). EDLCs have already been used as memory back-up devices for almost a decade. The capacitive behavior of carbon materials can be further improved by the presence of active species that contribute to the total specific capacitance by the pseudocapacitive effect.[3] Active species such as metal oxides[4,5] or conducting polymers[6,7] can be reversibly oxidized/reduced over the potential range of operation. Heteroatoms and functional groups present in a carbon matrix change the electron/donor characteristics of the carbon electrode material.[8] It has been assumed that nitrogen functionalities change the electron donor/acceptor characteristics of carbon depending on the type of the groups formed between the nitrogen and carbon atoms.[9] Jurewicz et al. reported on the improvement of supercapacitor performance of activated carbon subjected to the ammoxidation process.[10] The acid−basic properties of cellulose-derived activated carbon were changed after the incorporation of nitrogen and oxygen species by ammoxidation, resulting in the increase of the gravimetric specific capacitance. In this paper, we report on the electrochemical performance of supercapacitors prepared from melamine-based carbon. For the first time, we have manufactured the capacitors from carbon derived from melamine prepared by a template method. Because the melamine resin contains 45 wt % of nitrogen, we believed it to be a promising candidate for the synthesis of a nitrogen-rich carbon electrode material for supercapacitors. In addition, melamine is a commercially available and very cheap polymer. Several reports on the preparation of advanced carbon materials from melamine are available currently. For instance, Bagreev at al. prepared nitrogen-containing coal-based activated carbon from bituminous coal and melamine.[11]

* To whom correspondence should be addressed. Tel.: +81-29-861-8430. Fax: +81-29-861-8408. E-mail: denisa-hulicova@aist.go.jp.

(1) Shiraishi, S.; Kurihara, H.; Shi, L.; Nakayama, T.; Oya, A. *J. Electrochem. Soc.* **2002**, *149*, A855.
(2) Lewandowski, A.; Zajder, M.; Frackowiak, E.; Beguin, F. *Electrochim. Acta* **2001**, *46*, 2777.
(3) Conway, B. E. *Electrochemical Supercapacitors: Scientific Fundamentals and Technological Applications*; Kluwer-Plenum Press: New York, 1999.
(4) Kim, H.; Popov, B. N. *J. Power Sources* **2002**, *104*, 52.
(5) Hu, C. C.; Wang, C. C. *Electrochem. Commun.* **2002**, *4*, 554.
(6) Chen, W.; Wen, T.; Teng, H. *Electrochim. Acta* **2003**, *48*, 641.
(7) Ingram, N. D.; Pappin, A. J.; Delalande, F.; Poupard, D.; Terzulli, G. *Electrochim. Acta* **1998**, *43*, 10601.
(8) Wu, Y. P.; Rahm, E.; Holze, R. *Electrochim. Acta* **2002**, *47*, 3491.
(9) Koh, M.; Nakajima, T. *Carbon* **2000**, *38*, 1947.
(10) Jurewicz, K.; Babel, K.; Ziolkowski, A.; Wachowska, H. *Electrochim. Acta* **2003**, *48*, 1491.
(11) Bagreev, A.; Angel Menendez, J.; Dukhno, I.; Tarasenko, Y.; Bandosz, T. J. *Carbon* **2004**, *42*, 469.

10.1021/cm049337g CCC: $30.25
Published on Web 01/29/2005

Such a material showed a hydrogen sulfide removal capacity exceeding more than 10 times the capacity of the material without melamine. Another nitrogen-containing activated carbon for application in catalysis was prepared from petroleum pitch and melamine resins.[12] A ferrocene/melamine mixture was used in the preparation of high-density aligned carbon nanotubes with uniform diameters.[13] Another report by Wang et al. describes the preparation and the thermoelectric power of nitrogen-doped carbon nanotubes when melamine was used as a starting material.[14] Furthermore mesoporous carbon aerogels doped with nitrogen atoms were also successfully synthesized from melamine and formaldehyde.[15,16] In addition, melamine was also used in the preparation of nitrogen-rich B−C−N materials.[17] Not only as carbon materials, but also in the polymeric state, the melamine-formaldehyde resins are very interesting materials for adsorption of various organic substances.[18,19] Melamine-based carbon has been already studied as an anode material for a lithium secondary battery.[20−22] It was shown that melamine-derived nitrogen-containing carbons further enriched with other agents, such as phosphorus or vanadium oxide, offer an increase in the reversible capacity of lithium storage and the enhancement of the cycling behavior.

We were particularly interested in the electrochemical behavior of nitrogen-enriched carbon derived from melamine manufactured as the electrode material in supercapacitors. Melamine was polymerized in the interlayer space of fluorine mica, and the pure nitrogen-enriched carbon was obtained after carbonization and mica removal. The mica was expected to introduce a layerlike structure and a certain degree of order into the resultant carbon material. The electrochemical characteristics of the prepared samples are discussed with respect to their porosities and elemental compositions.

Experimental Section

Materials. Melamine (2,3,6-triamino-1,3,5-triazine, Kanto Chemicals Co., Inc., purity 98%) and expandable fluorine mica were used as starting materials. The synthesis of fluorine mica can be found elsewhere.[23] The melamine/mica composite was prepared through the polymerization of melamine in the interlayer spaces of mica in formaldehyde in the ratio of melamine/mica/formaldehyde = 3/1/8 by weight. Polymerization took place at pH ≈ 9.1 and temperatures of 80 °C for 0.5 h under intensive stirring. After being dried at 60 °C in a conventional oven, samples were carbonized in an infrared furnace under flowing nitrogen and temperatures of 650, 750, 800, 850, and 1000 °C, heating rate 10 °C/min, and holding period of 1 h. Each sample was also stabilized in air at 250 °C for 4 h prior to carbonization. Samples subjected to no stabilization process are hereafter denoted as Me650, Me750, Me800, Me850, and Me1000. Their stabilized counterparts are termed Me650s, Me750s, Me800s, Me850s, and Me1000s.

Structural and Elemental Characterization. The elemental analysis was done by a conventional CHN combustion method (CHN, Yanako, Inc. Japan) based on the burnoff of the sample and TCD analysis of nitrogen and carbon mass percentage from the evolved gases.

X-ray photoelectron spectroscopy (XPS, ESCA 5600, Ulvac-Phi, Inc. Japan) was used in the surface analyses of the samples. Powdered samples were deposited on the sample holder and transferred into the XPS. Mg Kα line (15 kV, 30 mA, 400 W) was used as an X-ray source, and the C_{1s} peak position was set at 284.6 eV and taken as an internal standard. The peak separations of the N_{1s} core level peaks were estimated by least squares with Gaussian−Lorentzian product function using the Grams/386 software.

The surface morphologies of Me750 and Me750s were observed by field-emission scanning electron microscopy (JEOL S-4700, operated at 1.5 kV).

To characterize the pore structure, a nitrogen adsorption/desorption measurement at 77 K was conducted in a Belsorp18, Bel Japan, Inc. instrument. The α_s plots were created by the use of the standard adsorption isotherm of the nonporous carbon black (Mitsubishi No. 32).[24] The surface areas, micropore and mesopore volumes, as well as micropore and mesopore widths were then determined by the subtracting pore effect (SPE) method that has been proved to be an effective method because it removes enhanced effects by both the micropore filling and the quasi-capillary condensation.[25]

Electrochemical Measurements. Pellets for the electrochemical measurement were prepared by mixing the carbonized sample with carbon black (Mitsubishi Chemicals, Inc.) and poly(tetrafluoroethylene) binder (PTFE, Mitsui Dupont Fluorochemicals, 7A-J, Inc.). The ratio of sample:CB:PTFE was 80:10:10 wt %. Ammonium hydrocarbonate was added in a ratio of sample:NH_4HCO_3 = 1:1 by weight. NH_4HCO_3 was expected to form small pores in a pellet during its decomposition in the drying process (110 °C in a vacuum), and such pores should help the electrolyte diffusion. The final pellet weight was set at ca. 20 mg. Cyclic voltammmetry (CV) and galvanostatic charge/discharge cycling (GC) were employed in the evaluation of capacitance of each sample. Both CV and GC experiments were carried out at room temperature under flowing nitrogen in a standard three-compartment cell, when platinum foil and Ag/AgCl were used as the counter and the reference electrode, respectively. 1 M H_2SO_4 and 3 M NaCl were used as the electrolytes.

GC with the current loading of 20 mA g^{-1} was conducted on a multichanel VMP potentiostat/galvanostat (Multichannel potentiostats/galvanostats VMP-80, Princeton Applied research) in the potential range from −0.2 to 0.5 V versus Ag/AgCl. The specific gravimetric capacitance was calculated from the discharge process of the third cycle in a potential range of 0.2−0.1 V based on eq 1:

$$C_g = i\Delta t/\Delta V \quad (1)$$

(12) Raymundo-Pinero, E.; Cazorla-Amoros, D.; Linares-Solano, A.; Find, J.; Wild, U.; Schlogl, R. *Carbon* **2002**, *40*, 597.
(13) Cao, P. J.; Gu, Y. S.; Liu, H. W.; Shen, F.; Wang, Y. G.; Zhang, Q. F.; Wu, J. L.; Gao, H. J. *J. Mater. Res.* **2003**, *18*, 1686.
(14) Sadanadan, B.; Savage, T.; Bhattacharya, S.; Tritt, T.; Cassell, A.; Meyyappan, M.; Dai, Z. R.; Wang, Z. L.; Zidan, R.; Rao, A. M. *J. Nanosci. Nanotechnol.* **2003**, *3*, 99.
(15) Matsuoka, T.; Hatori, H.; Kodama, M.; Yamashita, J.; Miyajima, N. *Carbon* **2004**, *42*, 2329.
(16) Zhang, R.; Lu, Y.; Zhan, L.; Liang, X.; Wu, G.; Ling, L. *Carbon* **2002**, *411*, 1660.
(17) Popov, C.; Saito, K.; Yamamoto, K.; Ouchi, A.; Nakamura, T.; Ohana, Y.; Koga, Y. *J. Mater. Sci.* **1998**, *33*, 1281.
(18) Derylo-Marczewska, A.; Goworek, J.; Kusak, R.; Zgrajka, W. *Appl. Surf. Sci.* **2002**, *195*, 117.
(19) Goworek, J.; Derylo-Marczewska, A.; Stefaniak, W.; Zgrajka, W.; Kusak, R. *Mater. Chem. Phys.* **2002**, *77*, 276.
(20) Wu, Y.; Fang, S.; Jiang, Y. *J. Power Sources* **1998**, *75*, 167.
(21) Wu, Y.; Fang, S.; Jiang, Y. *J. Mater. Chem.* **1998**, *8*, 2223.
(22) Wu, Y. P.; Wan, C. R.; Li, Y.; Fiang, S.; Jiang, Y. *Electrochem. Solid-State Lett.* **1999**, *2*, 118.
(23) Tateyama, H.; Nishimura, S.; Tsunematu, K.; Jinnai, K.; Adachi, Y.; Kimura, M. *Clays Clay Miner.* **2002**, *23*, 180.
(24) Gregg, K. S. J.; Sing, K. S. W. *Adsorption Surface Area and Porosity*; Academic Press: New York, 1982.
(25) Setoyama, N.; Suzuki, T.; Kaneko, K. *Carbon* **1998**, *36*, 1459.

Table 1. N/C Ratios of Nonstabilized and Stabilized Samples Evaluated from CHN and XPS, and Carbon Yields of All Samples

sample	N/C_{CHN}	N/C_{XPS}	yield [wt %]
Me650	0.37	0.22	30.37
Me750	0.24	0.20	25.71
Me800	0.24		24.20
Me850	0.20	0.21	23.26
Me1000	0.08	0.11	20.86
Me650s	0.45	0.45	41.58
Me750s	0.43	0.34	39.40
Me800s	0.41		36.57
Me850s	0.32	0.25	34.89
Me1000s	0.13	0.14	30.38

where C_g is the specific gravimetric capacitance (F g^{-1}), i is the current loaded (20 mA g^{-1} in this study), Δt is the change of the negative process duration in the evaluated region (s), and ΔV is the potential change during the negative process (0.1 V in this study).

Specific capacitances per surface area C_{SA} (F m^{-2}) were also calculated using eq 2:

$$C_{SA} = C_g/SA \tag{2}$$

where SA is a total surface area (m^2 g^{-1}) calculated from the α_s plots.

CV was performed with the same cell layout under the following conditions: potential scan rate of 0.1 mV s^{-1} and potential range of 0−0.5 V.

Results and Discussion

Table 1 shows the N/C ratios evaluated from the CHN elemental analysis, the N/C ratio determined from XPS analysis, and the carbonization yield of each sample. The nitrogen content reasonably decreases with the heat-treatment temperature for both the nonstabilized and the stabilized groups of samples. In the case of the nonstabilized samples, the highest N/C ratios are detected in Me650 as 0.22 and 0.37 from CHN and XPS, respectively. On the other hand and as expected, Me1000 contains the least nitrogen among the nonstabilized samples, 0.11 and 0.08 from CHN and XPS, respectively. The stabilized samples, however, contain moderately higher amounts of nitrogen than the nonstabilized ones; for example, N/C of Me650s and Me1000s are 0.45 (from XPS and CHN) and 0.13 (0.14) from CHN (XPS), respectively. This indicates that the stabilization process was very effective in "capturing" the nitrogen atoms in a carbon matrix and therefore Me1000s still contains a moderate amount of nitrogen despite the relatively high heat-treatment temperature. It is also noticeable that the main release of nitrogenous volatiles occurred at temperatures higher than 850 °C. The chemical state of nitrogen will be discussed later on the basis of XPS analysis.

The safety emission of volatiles during the carbonization was precisely controlled. The volatiles were delivered directly from the furnace via the laboratory draft chamber to the central draft chamber. There the evolved gases passed through a high-efficient filtration system and the nonharmful gaseous products were finally released.

The carbon yields (Table 1) become lower with the heat-treatment temperature in nonstabilized samples; for example, the carbon yields of Me650 and Me1000 are 30.37% and 20.96%, respectively. Stabilized samples provide higher carbonization yields, 41.58% and 30.38 wt % for Me650s and Me1000s, respectively. Hence, the stabilization process was an important procedure not only for the increase of the amount of nitrogen but also the carbon yield.

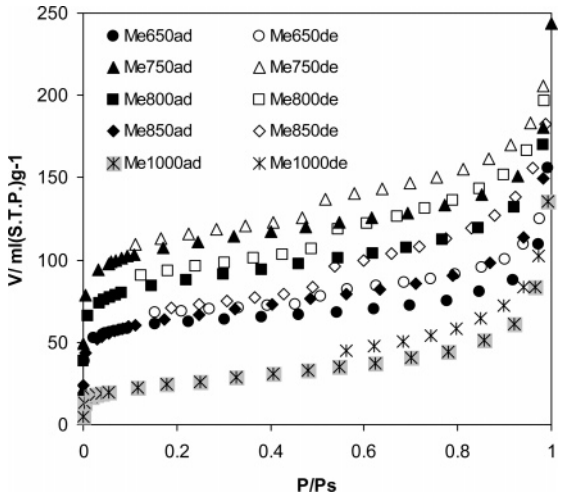

Figure 1. N_2 adsorption/desorption isotherms of nonstabilized samples. Solid and open symbols represent adsorption and desorption isotherms, respectively.

Table 2. Surface Areas, Total Pore Volumes, Micropores Volumes, Mesopores Volumes, Mean Micropores Widths, and Mesopores Widths for Nonstabilized and Stabilized Samples[a]

sample	$SA_{\alpha s}$ [m^2 g^{-1}]	V_{total} [mL g^{-1}]	V_{micro} [mL g^{-1}]	V_{meso} [mL g^{-1}]	w_{micro} [nm]	R_{meso} [nm]
Me650	260	0.24	0.08	0.16	0.72	8.7
Me750	442	0.38	0.13	0.25	0.73	5.9
Me800	345	0.41	0.09	0.31	0.95	4.0
Me850	248	0.35	0.06	0.29	0.73	6.8
Me1000	86	0.21	0.01	0.20	0.80	6.5
Me650s	138	0.25	0.03	0.22	0.58	12.1
Me750s	256	0.32	0.07	0.25	0.74	7.5
Me800s	202	0.27	0.05	0.22	0.78	6.0
Me850s	120	0.24	0.02	0.22	0.71	6.9
Me1000s	17	0.17		0.15		4.3

[a] All values were calculated by the SPE method.

The porous nature of all of the samples was further investigated by a nitrogen adsorption/desorption measurement, and resultant N_2 adsorption and desorption isotherms of nonstabilized samples are shown in Figure 1. The surface areas (SA), total pore volumes (V_{total}), micropore volumes (V_{micro}), mesopore volumes (V_{meso}), micropore widths (w_{micro}), and mesopore widths (R_{meso}) of all samples are listed in Table 2. Taking into account the total amount of nitrogen adsorbed, it can be said that the porosities in all of the samples are not developed very much. This is a reasonable conclusion as no activation process was used. Among the nonstabilized samples, Me750 adsorbs the highest amount of nitrogen and therefore it is the sample with the highest porosity (SA = 442 m^2 g^{-1}). The adsorption of N_2 is observed at low relative pressure due to the micropore-filling effect. The adsorption gradually increases in the region of middle P/P_s and further in the region of high pressure >0.8 P/P_s. Such adsorption behavior can be attributed to the capillary condensation of nitrogen in the mesopores or macropores and multilayer adsorption of mesopores or macropores. Thus, it can be concluded that this sample contains micropores together with the meso- and/or macropores. The adsorption/desorption

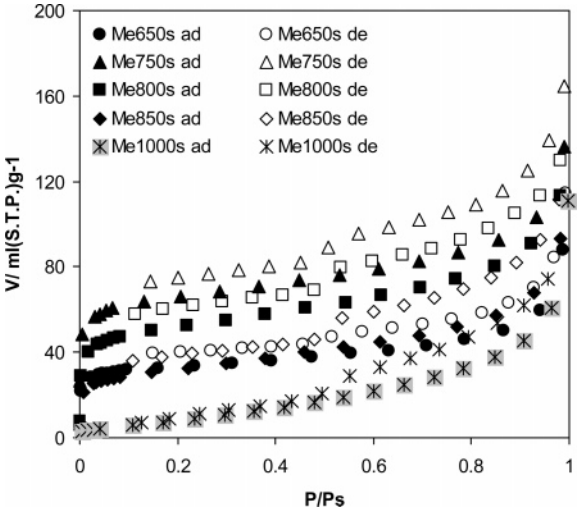

Figure 2. N_2 adsorption/desorption isotherms of stabilized samples. Solid and open symbols represent adsorption and desorption isotherms, respectively.

isotherms of other samples have similar shapes, indicating the same presence of a mixture of micropores and mesopores (or macropores); however, the total amounts of nitrogen adsorbed are lower. The surface areas decrease with the heat-treatment temperature (HTT), reaching the minimum of 86 $m^2\ g^{-1}$ for Me1000. On the other hand, the surface area of Me650 is also smaller than that of Me750, probably because the temperature of 650 °C was not sufficient for the release of all decomposable species. As for the V_{micro}, the highest value is observed in Me750 and it gradually decreases with the HTT. Again, the V_{micro} for Me650 is smaller than that for Me750 due to the smaller surface area. However, w_{micro} does not change significantly with the HTT, and the widest micropores of 0.95 nm are detected in Me800. The mesopore contribution to the total pore volume (V_{total}) is significant in the samples heat-treated at higher temperatures, for example, Me850 and Me1000. Reasonably, the lowest contribution of mesopores to V_{total} is in Me750, which is the sample with the highest surface area and V_{micro}. The widest mesopores are detected in Me650 with an R_{meso} of 8.7 nm.

Figure 2 shows the N_2 adsorption and desorption isotherms of the stabilized samples. It is obvious that these samples adsorb less nitrogen than the nonstabilized ones and that they are less porous. Me750s is again the sample with the highest SA among the stabilized sample (SA = 256 $m^2\ g^{-1}$); however, the surface area is reduced significantly. As for the Me1000s, the surface area decreases dramatically to 17 $m^2\ g^{-1}$, and a similar reduction can be observed for each stabilized sample. The reason for that must be the stabilization process during which the sample melted and shrunk. Therefore, the release of gases during the carbonization process could not form pores to the same extent as in the nonstabilized samples. The micropore volumes in the stabilized samples are reasonably lower (Table 2). On the other hand, the mesopores become slightly larger with the stabilization process; for example, the R_{meso} of Me650s is 12.1 nm. Considering the mesopore volumes, it is clear that the mesopores contribute significantly to the total pore volume V_{total} in the stabilized samples.

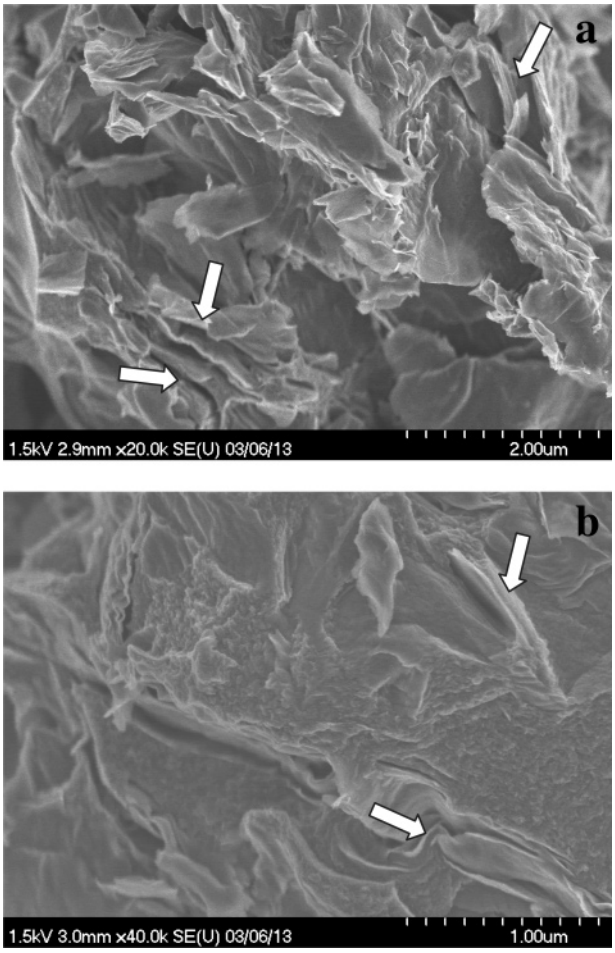

Figure 3. FE-SEM photographs of Me750 (a) and Me750s (b). A layerlike structure can be observed in both of the samples, although Me750s is denser.

SEM photographs of Me750 and Me750s are shown in Figure 3. A quasi layerlike structure, indicated by the arrows, can be observed, although the stabilized Me750s sample appears to be denser. This is in accordance with the adsorption behavior of these samples discussed above. The layerlike structure proves that melamine polymerized in the interlayer space of the mica.

The chemical state of nitrogen present in the carbonized samples is further discussed on the basis of the XPS results. Figure 4 shows the N_{1s} core level peaks of nonstabilized and stabilized samples. The fitting of the peaks for Me650 shows the existence of three contributions at binding energies of 398.7, 400.9, and 402.7 eV. These peaks can be assigned to pyridine (398.5 ± 0.2 eV), quaternary (401.2 ± 0.2 eV), and oxidized nitrogen (402.9 ± 0.2 eV), respectively.[10,12,26] The fitting of the N_{1s} core level peaks for Me750, Me850, and Me1000 shows three contributions at the same binding energies, however, with different relative contributions. The amount of quaternary nitrogen increases with the HTT, indicating the chemical change and transformation of nitrogen groups during the heat treatment. The amount of peripheral pyridine nitrogen decreases, whiles the proportion of quaternary nitrogen located within the graphene sheets increases. These results indicate that the pyridine nitrogen

(26) Stanczyk, K.; Dziembaj, R.; Piwowarska, Z.; Witkowski, S. *Carbon* **1995**, *33*, 1383.

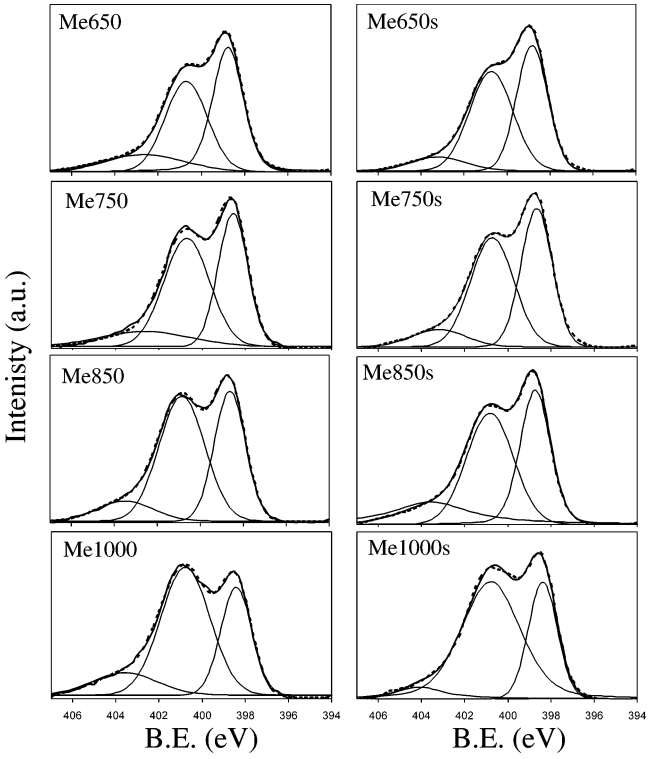

Figure 4. N_{1s} core level peaks of nonstabilized and stabilized samples.

Table 3. Ratios of Pyridinic (Np), Quaternary (Nq), and Oxidized (No) Nitrogen of All Samples Evaluated from the Peak Separation Analyses of N_{1s} Core Level Peaks

sample	Np (%) 398.5 ± 0.2 eV	Nq (%) 401.2 ± 0.2 eV	No (%) 402.9 ± 0.2 eV
Me650	53.7	38.9	7.4
Me750	51.9	42.2	5.9
Me850	47.3	45.3	7.4
Me1000	38.5	53.5	8.0
Me650s	54.6	39.6	5.8
Me750s	52.3	41.2	6.5
Me850s	49.8	43.3	6.9
Me1000s	43.3	51.4	5.3

has been chemically transformed into nitrogen species with higher binding energies through the condensation reactions occurring during carbonization. The peak analyses of N_{1s} for the stabilized samples revealed the presence of the same three contributions, but with different contributions. The ratios of pyridinic, quaternary, and oxidized nitrogen for all samples are summarized in Table 3. The main conclusion of the peak deconvolution analysis is that the stabilized samples contain slightly larger amounts of pyridinic nitrogen as compared to their nonstabilized counterparts. In addition, for both the stabilized and the nonstabilized samples heat-treated at higher temperatures, the shifting of the oxidized nitrogen binding energies to the higher values can be noticed. Hence, the XPS results suggest that the surface functionalities and the capacitive performance of both the stabilized and the nonstabilized samples may be considered further.

The electrochemical behaviors of all of the samples in 1 M H_2SO_4 are discussed next. The specific gravimetric capacitances (C_g) and specific capacitances per surface areas (C_{SA}) evaluated from the GC measurements are summarized in Table 4.

To avoid the influence of oxygen, all calculations are done from the discharge process of the third cycle. Concerning the C_g of nonstabilized samples, it is remarkable that the values are unexpectedly high with respect to the low porosities. It can be seen that the capacitance increases with HTT reaching the maximum of 204.8 F g^{-1} for Me750. It should be reminded that this sample has the highest specific surface area among the nonstabilized samples (SA = 442 m^2 g^{-1}) and a high ratio of nitrogen (N/C = 0.24). The further increase of the carbonization temperature causes the capacitance to decrease down to the minimum of 47.92 F g^{-1} for Me1000. This is the sample with the lowest specific surface area (SA = 86 m^2 g^{-1}) and the lowest ratio of nitrogen (N/C = 0.08). The gravimetric capacitances of the stabilized samples are close to their nonstabilized counterparts despite the remarkably lower surface areas. Again, the sample heat-treated at 750 °C ($Me750_s$) is the sample with the highest SA (256 m^2 g^{-1}) and the best gravimetric capacitive performance (C_g = 200.1 F g^{-1}). As expected, $Me1000_s$ as an almost nonporous sample with a SA = 17 m^2 g^{-1} has the poorest gravimetric capacitance (C_g = 62.24 F g^{-1}). Considering the above results, one may conclude that the gravimetric capacitance of the stabilized and nonstabilized samples depends on the nitrogen content and the porosity, that is, the higher the nitrogen content and the porosity, the better the capacitive behavior. However, this thought should be reconsidered if the capacitance is interpreted as the specific capacitance per surface area. In this case, the samples with the poor SA provide high values of specific capacitance per surface area (Table 4). Concerning the nonstabilized samples, the C_{SA} values of all of the samples are similar or very close. Me750 is even the sample with the lowest value of C_{SA} among the nonstabilized samples (0.46 F m^{-2}), and Me850 is a sample with the best capacitive performance (0.63 F m^{-2}).

On the other hand, the C_{SA} values of the stabilized samples are generally higher than those of the nonstabilized ones. This is quite reasonable because the stabilized samples are less-porous while providing high values of C_g. Me750s is the sample with the lowest C_{SA} (0.78 F m^{-2}); however, it is still a higher value if compared to nonstabilized Me750. The best capacitive performance per surface area was measured for Me1000s that is 3.66 F m^{-2}. This is a sample with almost no porosity (SA = 17 m^2 g^{-1}) and the lowest amount of nitrogen (N/C = 0.14).

These results clearly suggest a relationship between the nitrogen content, surface area, and the electrochemical capacitance, which is not linear. Considering the surface area and the capacitive behavior, some authors believe that the relationship between the specific surface area and the electric double layer capacitance of carbon is proportional.[3,27] However, other researchers report on a nonlinearity between surface area of carbon and double layer capacitance.[1,28]

Chronopotentiographs of the nonstabilized and stabilized samples are shown in Figure 5a and b, respectively. Significant IR drops reflecting the poor conductivity and large resistance of the electrode carbon materials can be

(27) Morimoto, T.; Hiratsuka, K.; Sanada, Y.; Kurihara, K. *J. Power Sources* **1996**, *60*, 239.
(28) Yoon, S.; Lee, J.; Hyeon, T.; Oh, S. M. *J. Electrochem. Soc.* **2000**, *147*, 2507.

Table 4. Specific Gravimetric Capacitances (C_g) and Specific Capacitances Per Surface Area (C_{SA}) of All Samples in 1 M H_2SO_4[a]

	sample									
	Me650	Me750	Me800	Me850	Me1000	Me650s	Me750s	Me800s	Me850s	Me1000s
C_g [F g^{-1}]	141.1	204.8	198.8	157.4	47.92	128.2	200.1	185.6	195.9	62.24
C_{SA} [F m^{-2}]	0.54	0.46	0.57	0.63	0.55	0.93	0.78	0.92	1.63	3.66

[a] Calculations were done from the discharge process of the third cycle in the potential range of 0.2−0.1 V. Surface areas were estimated by the SPE method.

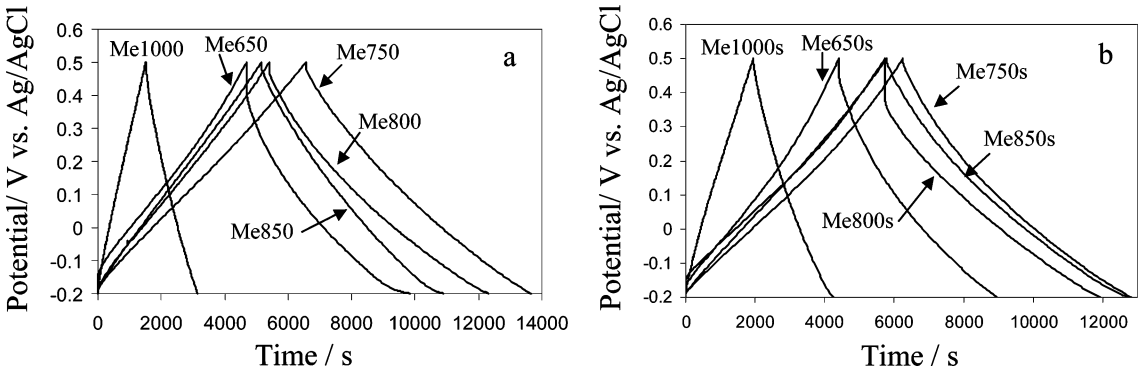

Figure 5. Potential−time curves (chronopotentiographs) for nonstabilized samples (a) and stabilized samples (b). Galvanostatic conditions, 20 mA g^{-1}, potential range −0.2 to 0.5 V, vs Ag/AgCl.

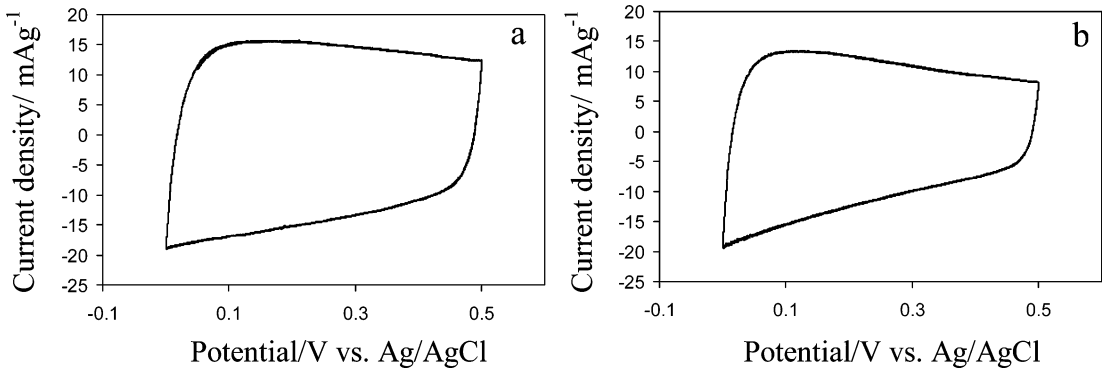

Figure 6. Cyclic voltammograms of the capacitors manufactured from Me750 (a) and Me750s (b). Voltammetric conditions, sweep rate 0.1 mV s^{-1}, potential range 0−0.5 V, vs Ag/AgCl.

observed in samples heat-treated at lower temperature of 650 °C, that is, Me650 and Me650s. Almost no IR drop can be detected in samples heated above this temperature, except for Me800s. The triangle shape for the chronopotentiographs of all of the samples heated above 650 °C proves their good capacitive behavior.

Cyclic voltammetry was also used in the determination of the electrochemical properties of the samples, and the example voltammograms for Me750 and Me750s are shown in Figure 6a and b. The shape of the voltammogram for Me750 is almost square, suggesting an electrostatic attraction. However, a slight slope in the region of proton electrosorption can be observed. This indicates some deviations from the ideal double-layer capacitor. Such features become more significant in Me750s, the voltammogram of which is not square and the slope of which is easily recognized. Because the scan rate was slow enough to eliminate kinetic effects during the sorption of ions, we suggest that this deviation is related to the pseudocapacitive properties of the present samples, which should be considered due to the presence of incorporated nitrogen in an appreciable amount. It was suggested previously that the pyridinic nitrogen at the periphery of the graphene layers provides a pair of electrons introducing electron donor properties to the layer.[9] The XPS study clearly shows the presence of pyridinic and quaternary nitrogen in all samples, while the pyridinic nitrogen ratios are slightly higher in the stabilized samples. These nitrogen species are located at the easily accessible edges of graphene layers, and therefore they can easily contribute to the total capacitance with the pseudocapacitive effect. As mentioned previously, pyridinic nitrogen induces electron donor properties to the layer, and therefore one can reasonably assume that the protons were attracted to the electrode surface and the pseudocapacitive interactions occurred. This may be a reason for the good capacitive properties of stabilized samples with very poor porosities but with the higher ratios of pyridinic nitrogen as compared to the nonstabilized samples.

To further investigate the theory of proton involvement in the charge−discharge process, we have changed the pH of aqueous electrolyte, and 3 M sodium chloride (NaCl) was used instead of 1 M H_2SO_4. The C_g and C_{SA} evaluated from the galvanostatic charge/discharge measurements of Me750, Me750s, Me1000, and Me1000s are summarized in Table

Table 5. Specific Gravimetric Capacitances (C_g) and Specific Capacitances per Surface Area (C_{SA}) of All Samples in 3 M NaCl[a]

sample	C_g [F g^{-1}]	C_{SA} [F m^{-2}]
Me750	74.29	0.17
Me750s	59.85	0.23
Me1000	20.85	0.24
Me1000s	15.74	0.93

[a] Calculations were done from the discharge process of the third cycle in the potential range of 0.2−0.1 V. Surface areas were estimated by the SPE method.

5. Unlike the C_g measured in acidic medium, the C_g in NaCl decreases with the surface areas, and the stabilized samples provide lower C_g than the nonstabilized ones, regardless of the nitrogen contents. The highest C_g (74.29 F g^{-1}) was obtained from Me750. This is, however, almost 3 times less than the gravimetric capacitance of this sample in sulfuric acid (204.8 F g^{-1}). A further capacitance loss is observed in all other samples, that is, 59.85 F g^{-1} in Me750s, 20.85 F g^{-1} in Me1000, and 15.74 F g^{-1} in Me1000s. Considering the capacitive performances of the samples with respect to their porosities, the C_{SA} values of Me750, Me750s, and Me1000 are close to the C_{SA} of activated carbon, which is usually between 0.1 and 0.2 F m^{-2}. Therefore, we suggest that the capacitance in NaCl originates in a mainly non-Faradaic electrostatic sorption of ions on the double layer. The high C_{SA} values of Me1000s in both electrolytes, that is, 3.66 F m^{-2} in H_2SO_4 and 0.93 F m^{-2} in NaCl, are not clarified yet, and further investigation of this sample is in progress. However, in general, the results presented suggest the proton involvement in the charge−discharge process in acidic medium and the mainly electrostatic sorption of ion in a neutral medium.

Conclusions

For the first time, novel supercapacitors were manufactured from melamine-based carbons prepared by a template method using fluorine mica as template. It was observed that samples subjected to nonstabilization process had a better developed porous structure as compared to the stabilized samples and that they contained micropores together with meso- and macropores. The CHN combustion method and XPS revealed a higher nitrogen content in the stabilized samples with the maximum and minimum of N/C = 0.45 and N/C = 0.14 for Me650s and Me1000s, respectively. The stabilization process was effective not only for the preparation of samples with higher nitrogen content, but also for the increment of carbon yield. N_{1s} peak analyses of all samples revealed that the main nitrogen species were pyridinic, quaternary, and oxidized nitrogen and that the stabilized samples contained slightly higher ratios of pyridinic nitrogen located at the periphery of the graphene sheets. The results of the electrochemical measurements of capacitors built from each sample in sulfuric acid suggested the presence of pseudocapacitive effect due to the active nitrogen sites. This became more significant in the stabilized samples that generally provided high values of capacitances despite the lower surface areas. The pseudocapacitive interaction was not observed when a neutral electrolyte was used. Hence, we suggested that the pyridinic nitrogen species affected the electron donor−acceptor characteristic of carbon materials and that the pseudocapacitive attraction between the protons of electrolyte and the carbon electrode materials occurred. This was stated to be the reason for good capacitive behavior of melamine-based carbon in sulfuric acid. To understand the origin of pseudocapacitance more precisely, further investigation is in progress.

Acknowledgment. D.H. is grateful to the Japan Society for Promotion of Science (JSPS) for financial support.

CM049337G